

Characteristics of charge density waves on the surfaces of quasi-one-dimensional charge-transfer complex layered organic crystals

Feng Lin,¹ Xiaoming Huang,³ Shengchun Qu,⁴ Zheyu Fang,¹ Shan Huang,¹ Wentong Song,¹ Xing Zhu,^{1,2,*} and Zhongfan Liu³

¹*School of Physics and State Key Laboratory for Mesoscopic Physics, Peking University, Beijing 100871, China*

²*National Center for Nanoscience and Technology, 100190 China*

³*Center for Nanochemistry, Beijing National Laboratory for Molecular sciences (BNLMS), State Key Laboratory for Structural Chemistry of Unstable and Stable Species, College of Chemistry and Molecular Engineering, Peking University, Beijing 100871, China*

⁴*Key Laboratory of Semiconductor Materials Science, Institute of Semiconductors, Chinese Academy of Sciences, Beijing 100083, China*

(Received 2 November 2010; published 31 March 2011)

We performed scanning tunneling microscope (STM) studies to observe the surface electronic structure of the following semiconducting charge-transfer complexes: dipropylamine-tetracyanoquinodimethane [DPA(TCNQ)₂], triethylammonium [TEA (TCNQ)₂], and *N*-ethylmorpholinium [HEM(TCNQ)₂], which all possess the molecularly flat *bc* surface terminated predominately with the quasi-one-dimensional (1D) TCNQ^{-0.5} anion chains or the corresponding DPA⁺, TEA⁺, and HEM⁺ cations contributing a lesser fraction. On the *bc* surfaces terminated with TCNQ^{-0.5} anions for all crystals, the $4k_F$ [DPA(TCNQ)₂] or $2k_F$ [TEA(TCNQ)₂ and HEM(TCNQ)₂] charge density wave (CDW) driven by the spin-Peierls or Peierls instability for the quasi-1D TCNQ^{-0.5} chains, respectively, which occur already within the bulk, were probed by use of STM on the crystal surfaces. In that the surface lattice constants obtained from CDW are in good agreement with the bulk ones obtained by x-ray diffraction, such CDWs are commensurate. This modulation of the electric structure is so distinct that the geometric corrugation of individual TCNQ anions was hardly traced during our STM measurements. On the *bc* surfaces terminated with DPA⁺, TEA⁺, and HEM⁺ cations, the STM images with submolecular resolution represent the geometric corrugation of individual molecular cations, and the surface lattice constants obtained deviate greatly from that of the x-ray crystal structures, indicating self-reassembling of the surface cations.

DOI: [10.1103/PhysRevB.83.125434](https://doi.org/10.1103/PhysRevB.83.125434)

PACS number(s): 68.65.-k, 73.20.At, 68.35.bg, 68.47.Fg

I. INTRODUCTION

Since the discovery of metallic conductivity in a charge-transfer (CT) complex, tetrathiafulvalene-tetracyanoquinodimethane (TTF-TCNQ),¹ the exploration of such low-dimensional organic conductors based on π -functional molecules has been the subject of intensive research.²⁻¹⁵ For example, hundreds of different CT complexes containing TCNQ have been synthesized, like the series of C(TCNQ)₂ with stoichiometry 1:2 (C denotes cation molecules) and quasi-one-dimensional (1D) TCNQ conducting chains in crystals, triethylammonium [TEA (TCNQ)₂],¹⁶ *N*-methyl-*N*-ethylmorpholinium [MEM (TCNQ)₂],¹⁷ dipropylamine [DPA(TCNQ)₂],^{18,19} *N*-ethyl-morpholinium [HEM(TCNQ)₂],²⁰ and so on. TCNQ is a very good electron acceptor for the presence of the four cyano groups and the relatively large π -electron conjugate system. As a result, in C(TCNQ)₂ crystals, every C molecule transfers one electron to two TCNQs, resulting in the C⁺ cation and TCNQ^{-0.5} anion. These crystals exhibit a wide variety of electrical conductivity, depending mainly on their structural form and cation properties. It was found mostly by x-ray diffraction^{16,17} that the crystalline structure of these C(TCNQ)₂ charge-transfer complexes usually exhibits a layered fashion in which layers of TCNQ anions alternate with layers of C cations, and in the TCNQ layer the TCNQ^{-0.5} form arrays of quasi-1D chains stacked by the overlapping of the π electrons of TCNQ. Arising from the special structural arrangement in crystals, these materials display a variety of novel electronic and magnetic properties, such as Peierls or spin-Peierls transitions, metal-insulator

transitions, magnetic-to-nonmagnetic transitions,¹⁶⁻¹⁹ and so on.

On crystallization during synthesis, the layers of C(TCNQ)₂ crystals tends to form large, molecularly flat crystal surfaces oriented to the layer direction, because of strong intermolecular in-plane interactions, especially the π - π overlapping interaction within the TCNQ chains. The large crystal surfaces naturally provide an appropriate arena for further practical applications in organic molecular devices²¹⁻²³ and to investigate the surface properties of organic crystals that have not been well studied so far in contrast to their inorganic counterparts, such as inorganic semiconductor crystals and metal crystals. Because the device properties usually strongly depend on the local arrangement of surface molecules, the surface structure at the submolecular level for these crystals are necessary to be clarified whether in fundamental or practical points of view. In the case of the the C(TCNQ)₂ crystals, there is little knowledge about surface features, such as step distribution, surface component, surface reconstruction and relaxation, and structural stability, etc., as the traditional inorganic semiconductors concerned. On the other hand, arrays of TCNQ chains in the TCNQ^{-0.5} layer for these C(TCNQ)₂ crystals are a quasi-1D system, which exhibit a $2k_F$ CDW structure driven by Peierls instability. It is of significant scientific interest to visualize the structural character of the TCNQ chains when they are exposed to surface. In this paper, we present the scanning tunneling microscope (STM) observations of the surface structures of the CT-complex crystals DPA(TCNQ)₂, TEA(TCNQ)₂, and HEM(TCNQ)₂. Using high-resolution STM images, we make clear the electronic and topographic structures of the

TCNQ^{-0.5} and the corresponding cation-terminated surfaces, respectively. In consideration of the interaction environments of the surface components that are bound by weak bonds (Van der Waals forces and hydrogen bonds), the surface structural stabilities are also evaluated on the basis of the obtained STM images.

II. EXPERIMENTAL METHOD

The CT-complex crystals TEA(TCNQ)₂, HEM(TCNQ)₂, and DPA(TCNQ)₂ were synthesized according to the method of Mebyl *et al.*²⁴ The following is the synthesizing process of the TEA(TCNQ)₂ crystal, which is taken as an example. First, the triethylammonium iodide was prepared by adding triethylamine into an HI solution. After filtration and drying at room temperature, a white crystal was obtained. A boiling solution of 0.204 g (1.0 mmol) of TCNQ (Aldrich, 98%) in 30 mL of acetonitrile was then mixed with a boiling solution of 0.115 g (0.5 mmol) of triethylammonium iodide in 5 mL of acetonitrile. The mixture solution with a dark green color was placed at room temperature for 48 h. Finally, by filtration, the black needlelike TEA(TCNQ)₂ crystals were collected.

These crystals were fixed onto a metallic plate with conductive silver epoxy, and it was then loaded into an ultrahigh vacuum chamber with a base pressure of about 3×10^{-10} mbar for STM measurements. The STM images were taken at room temperature, in a constant-current mode using a tunneling current of 0.3–0.5 nA and a bias voltage of 40–80 mV (with respect to the sample), otherwise stated therein. The STM tips used were mechanically cut from a wire of Pt(80%)Ir(20%) alloys. Lateral dimensions observed in the STM images were calibrated with a graphite standard.

III. RESULTS AND DISCUSSION

A. Crystal structures

Figures 1(a), 1(b), and 1(c) show the crystal structures of the CT complexes investigated here, TEA(TCNQ)₂, HEM(TCNQ)₂, DPA(TCNQ)₂, respectively, with the corresponding chemical structures in the lower part of each panel. The data used to construct the crystal unit-cell models were obtained from x-ray diffraction.^{16,18,20} The crystals all have a triclinic structure and $P\bar{1}$ symmetry, and their crystal parameters are listed in Table I. In Fig. 1(a), in a unit cell,

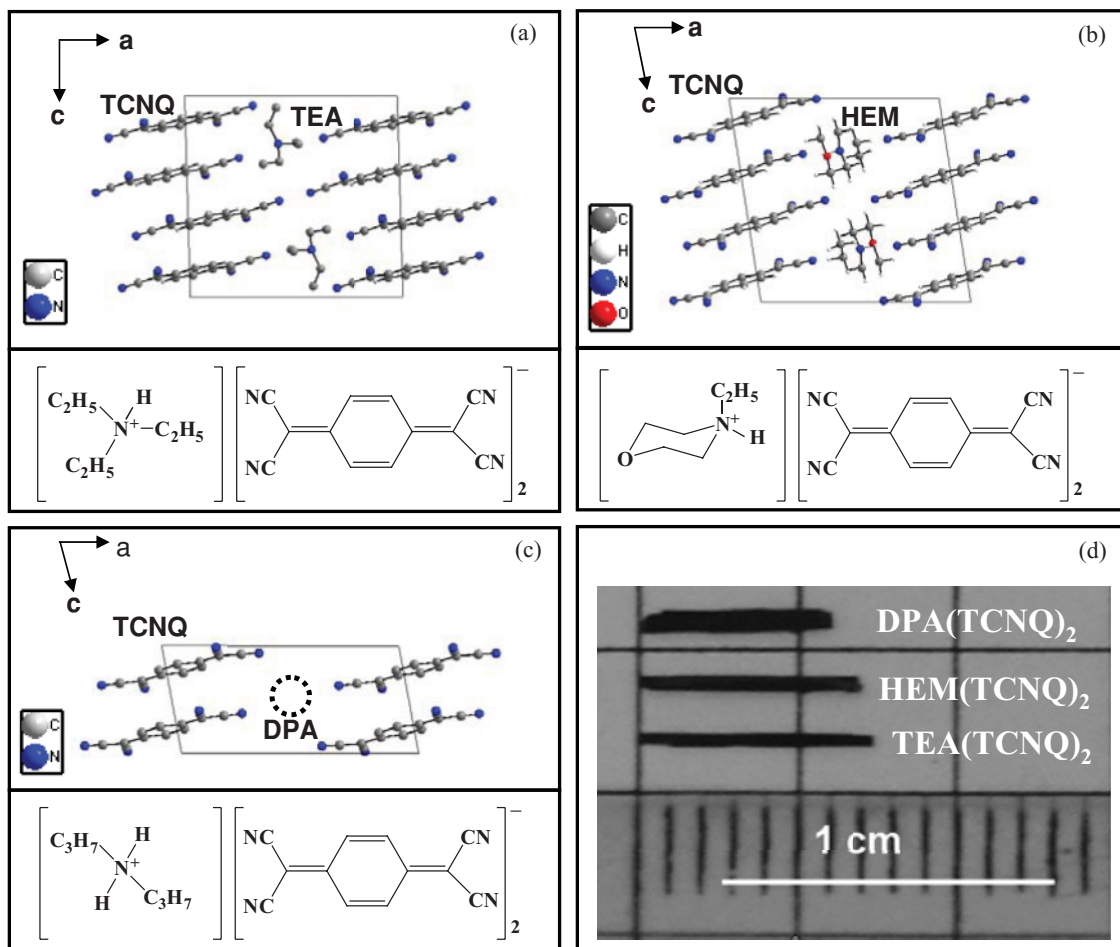


FIG. 1. (Color) [(a)–(c)] The crystal structures are shown in the upper paness and the chemical structures are shown in the lower panels for TEA(TCNQ)₂, HEM(TCNQ)₂, and DPA(TCNQ)₂, respectively. The crystal structures are represented with a ball-and-stick model. (d) Macroscopic aspects of the three organic crystals taken by a conventional optical microscope.

TABLE I. Lattice constants of the bc plane for DPA(TCNQ)₂, TEA(TCNQ)₂, and HEM(TCNQ)₂ determined from x-ray diffraction^a and STM^b.

Material	Space group	x-ray (Å)	STM ¹ (Å)	STM ² (Å)
		b	b	b
DPA(TCNQ) ₂	P-1	$b = 7.91$	$b = 8.4$	$b = 5.1, 7.0$
		$c = 6.56$	$c = 7.1$	$c = 10.0, 11.6$
		$\gamma = 84.0^\circ$	$\gamma = 80.1^\circ$	$\gamma = 85.7^\circ, 68.6^\circ$
TEA(TCNQ) ₂	P-1	$b = 7.89$	$b = 8.7$	$b = 10.2$
		$c = 13.22$	$c = 13.1$	$c = 7.7$
		$\gamma = 107.25^\circ$	$\gamma = 112.5^\circ$	$\gamma = 65.5^\circ$
HEM(TCNQ) ₂	P-1	$b = 7.56$	$b = 8.3$	$b = 8.7$
		$c = 13.42$	$c = 13.3$	$c = 7.3$
		$\gamma = 92^\circ$	$\gamma = 115.2^\circ$	$\gamma = 86.8^\circ$

^aThe x-ray data obtained from Refs. 14, 15 and 16.

^bSTM¹ refers to the bc plane terminated with TCNQ anions and STM² refer to the bc plane terminated with the corresponding cations.

the TCNQ anions form a tetrad of TCNQ^{-0.5} along the c axis, which is separated by TEA⁺ cations along the a axis, therefore the bc plane is composed of either arrays of TCNQ^{-0.5} chains or TEA⁺. This results in the alternating stacked structure of TCNQ layers and TEA layers in the bc plane. The interplanar spacings between two TCNQ^{-0.5}s within a tetramer are 3.24, 3.32, 3.24, and 3.30 Å, which all fall into the overlapping range of the π - π interaction. Therefore, the electron wave function along the c axis is delocalized. For more detail, the nearest-neighboring overlapping for TCNQ^{-0.5}s is the ring-external-bond and the shifted ring-external-bond types,¹⁶ resulting in molecular (geometric) corrugation of TCNQ^{-0.5} along the 1D chain (c axis).

The crystal structure of HEM(TCNQ)₂ is similar to that of TEA(TCNQ)₂, as shown in Fig. 1(b). The bc planes consist of of TCNQ^{-0.5} layers and HEM⁺ layers. The TCNQ^{-0.5}s repeated in a tetramer form chains along the c axis. Each tetramer is built up of two dimers related by an inversion center. The distance between TCNQ anions within a dimer is 3.23 Å; the intradimer overlap is of the ring-external-bond type. Within a tetramer the separation between the dimers is 3.31 Å and between successive tetramers 3.42 Å, with overlaps of the shifted ring-ring and ring-external-bond types, respectively.²⁰

In Fig. 1(c), the DPA(TCNQ)₂ crystal consists of alternately stacked TCNQ^{-0.5} and DPA⁺ layers along the a axis. In bc planes, the TCNQ^{-0.5} anions form a dimer unit within a chain along the c axis, with a ring-external-bond type. The distance between TCNQ^{-0.5}s is 3.27 Å. At room temperature, the DPA⁺ is disordered by the thermal motions, which thereby makes the location of DPA⁺ in the crystal model unable to be precisely defined through the x-ray diffraction data.¹⁸ The circle in Fig. 1(c) presents the approximate location of a DPA⁺.

Figure 1(d) presents the typical macroscopic aspects of the three crystals, taken by optical microscope. They are black, flake shaped, and elongated along the conductive c -axis direction. For all crystals, there always exists a smooth surface that is obviously much larger than other surfaces. By x-ray diffraction, this largest surface is determined to the bc plane.

B. Surface steps and terraces

For the three CT-complex crystals, the alternate layers are defined as the bc plane; therefore, in principle, the bc surface is either TCNQ^{-0.5} terminated or terminated by the corresponding cation. In STM observations, we found that most of the bc surface is terminated with TCNQ^{-0.5}, as expected, because of the strong intermolecular π - π interaction between TCNQ^{-0.5}s which significantly reduces the surface free energy. Occasionally, on some small terraces, the cations at the outmost surface were also found. For instance, Fig. 2(a) is a large-scale STM image of the bc surface for the TEA(TCNQ)₂ crystal, where large molecularly flat terraces hundreds of nanometers in size are identified as TCNQ^{-0.5} terminated,⁴ which will be verified in the latter text in the high-resolution STM images. Figure 2(b) is a cross-section profile measured along the A - B line. The height difference of larger neighboring terraces is about 1.45 nm, which is close to the lattice parameters in the direction of the a axis, 1.43 nm. Since a unit cell of the crystal consists of alternate TCNQ^{-0.5} and TEA⁺ layers stacked along the a axis, this step must be contributed from the two-layer height, both the TCNQ^{-0.5} and TEA⁺ layers. Identification of the two layers was clearly documented in our previous publication.⁴ The TEA⁺-terminated surface often appears in small terraces and occupies the smaller surface area. For example, a small terrace [marked in TEA in Fig. 2(a)] extends from a large terrace at the step edge, and the corresponding cross-section profile along the C - D line is shown in Fig. 2(c). Clearly, the TEA⁺ layer intervenes between two TCNQ^{-0.5} layers, with a height difference of 0.91 and 0.54 nm relative to the bottom and upper terraces, respectively. But the TEA⁺ layer in the crystal locates in the middle of the lower and upper TCNQ^{-0.5} layers on average. This difference from the surface TEA⁺ layer can be ascribed to the surface molecular relaxation.

The STM images in Fig. 3 were taken at a set-point tunneling current of 1.5 nA, which is much larger than the current (0.3–0.5 nA) normally used to scan the TEA(TCNQ)₂ crystal surfaces here. Figure 3(a) shows that during scanning, a layer of surface was suddenly removed under this high current, exhibiting a darker color in this region. A cross-section profile along A - B , shown in Fig. 3(b), indicates that the height of the disappeared layer is about 0.51 nm, which means that only the TCNQ layer was removed and the exposed surface then became TEA terminated. It is possible that a layer of TCNQ and a layer of TEA can be removed together, as shown in Figs. 3(c) and 3(d), where the height of the disappeared layers is about 1.41 nm, agreeing well with the height of the two layers in bulk (lattice constant in the a axis). The removing process induced by STM is not well understood, which may be pulled and pushed by the STM tip during scanning due to the large tip-sample interaction under the high tunneling current on this soft crystal surface. With this removed process, the desired surface, for example, the TCNQ^{-0.5}-terminated or TEA⁺-terminated surface, can be easily achieved.

C. Submolecular-resolution TCNQ^{-0.5}-terminated surfaces

Figure 4(a) shows a high-resolution STM image of the TCNQ^{-0.5} anions terminated bc surface for the DPA(TCNQ)₂ crystal at room temperature, where the characteristic bright

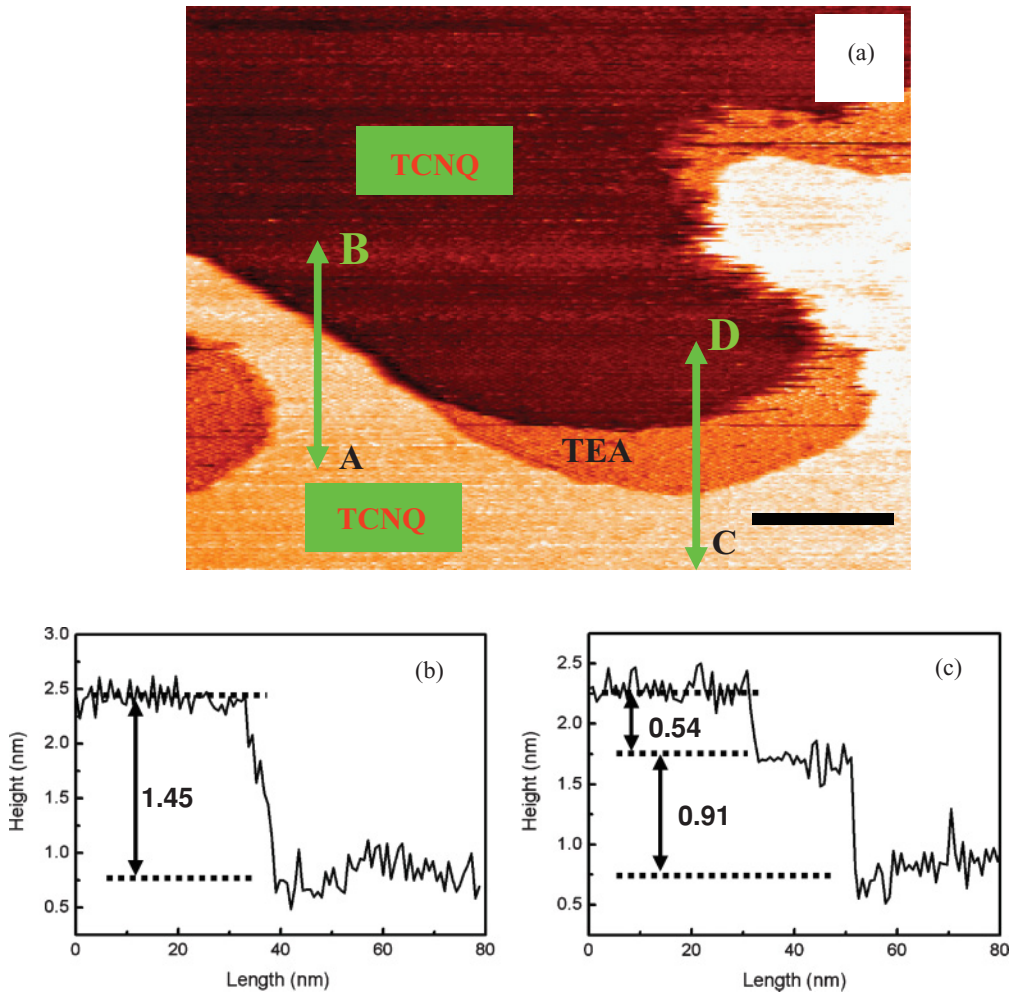


FIG. 2. (Color online) (a) Large-scale STM image of the *bc* surface for TEA(TCNQ)₂, which clearly shows surface steps and terraces. Scale bar = 52 nm. [(b) and (c)] Height profile along the lines of the AB and CD arrows in (a).

lobes appear as obvious periodicity. The unit cell drawn in the arrows is $b = 0.84$ nm, $c = 0.71$ nm, and $\gamma = 80.1^\circ$, which agrees with the crystal structure obtained by x-ray diffraction, $b = 0.79$ nm, $c = 0.66$ nm, and $\gamma = 84^\circ$. For clearer comparison in the crystallographic structure between the STM image and the corresponding x-ray diffraction result, Fig. 4(b) presents a space-filling model of the *bc* surface terminated with TCNQ^{-0.5}s constructed with the data of x-ray diffraction,¹⁸ and a row of TCNQs cut from the above STM image. The space-filling model shows only the arrays of TCNQ^{-0.5} chains on the outmost surface, and the individual TCNQ^{-0.5} anion is in the slightly tilted stand-upright form along the molecular long axis of TCNQ. From the STM image, we cannot distinguish the individual TCNQ^{-0.5} anion from the lobe. Through the size comparison [the red lines in Fig. 4(b)], obviously, each lobe in the STM image corresponds to a TCNQ^{-0.5} dimer on the surface.

Figures 5(a) and 5(b) show the high-resolution STM images for the TEA(TCNQ)₂ and HEM(TCNQ)₂ *bc* surfaces terminated with TCNQ^{-0.5}s, respectively, with the space-filling models displaying the TCNQ arrangement under the respective STM images. The crystallographic parameters measured from

the STM images are, $b = 0.87$ nm, $c = 1.31$ nm, and $\gamma = 112.5^\circ$ for TEA(TCNQ)₂ and $b = 0.83$ nm, $c = 1.33$ nm, and $\gamma = 115.2^\circ$ for HEM(TCNQ)₂, in which is consistent with the data listed in Table I obtained by x-ray diffraction. Although there is an obvious difference in appearance for the two STM images, each feature (bright lobes) in the two images corresponds to a TCNQ^{-0.5} tetramer by comparing the images and the space-filling models. It is worth noting that there exist two other distinct structures, the monomer and octamer structures, on the TCNQ^{-0.5} terminated *bc* surface of TEA(TCNQ)₂,⁴ which might result from the complex balance of all kinds of surface energy, such as surface free energy, terrace boundary free energy, and defect energy. But they are metastable and easily change to the tetramer structure, or are quite rare in appearance, and are out of consideration here.

Due to the weak coupling between the TCNQ chains by Van der Waals forces, it is reasonable to consider the electronic structure of the TCNQ^{-0.5}-terminated surfaces within the frame of a simple assemble of 1D TCNQ chains. For within a 1D TCNQ chain, since the TCNQs bind strongly each other by the π - π overlapping interaction, its electronic structure can be described as a linear combination of lowest unoccupied

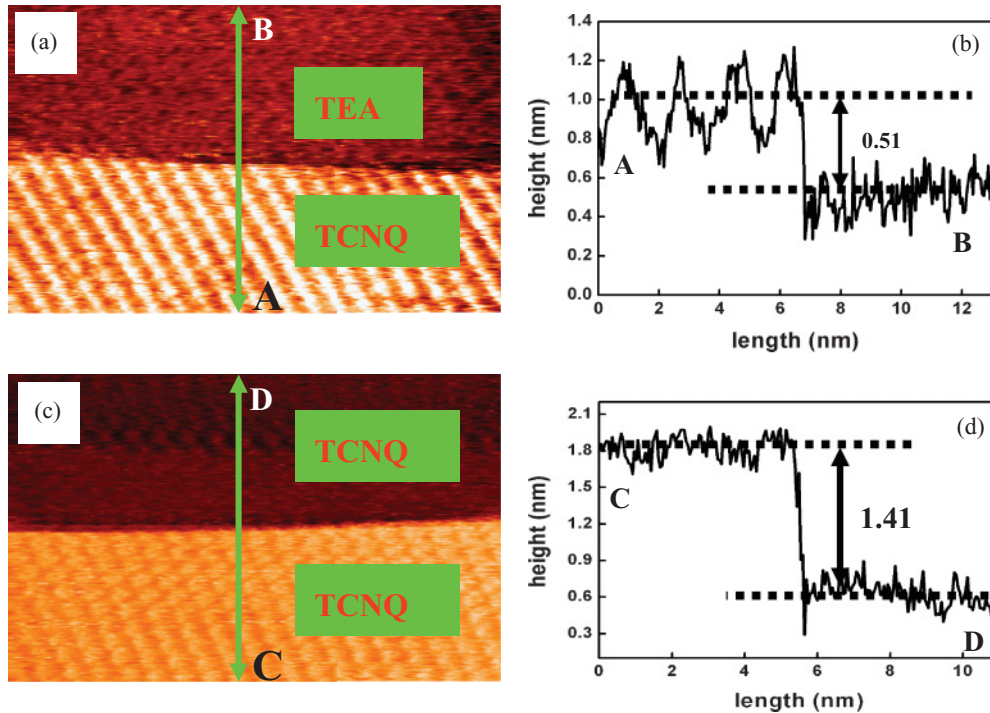


FIG. 3. (Color online) (a) [or (c)] STM image of the bc surface for TEA(TCNQ)₂ under a high-set-point current of 1.5 nA, about in the middle of which STM tip etching occurs, leading to a layer of TCNQ (or a layer of TCNQ and a layer of TEA) being removed. (b) [or (d)] Height profile along the double-headed arrow AB in (a) [or CD in (c)]. The scanning area of the two images is all $20 \times 12.5 \text{ nm}^2$.

molecular orbitals (LUMOs) of TCNQ. Figure 6(a) presents the LUMO of TCNQ, calculated based on the calculation of density functional theory, where the LUMO consists largely of contributions from the center phenyl ring with a lesser contribution from the outer nitrogen atoms. Since every TCNQ LUMO is partially occupied in the three crystals with $\rho = -0.5$ TCNQ sites (where ρ is the average electron per site), the highest occupied state (E_F , Fermi level) in the formed energy band can be achieved by electron filling. Interpretation of the STM images for the TCNQ^{-0.5}-terminated surfaces therefore is best described in terms of available states near E_F .

When every LUMO of TCNQ is occupied by 0.5 electrons, the energy band of the whole 1D chain is schematically shown in Figs. 6(b)–6(e), with the internal structure depending on the mutual relationship of the Coulomb repulsion energy (U) and the transfer integral (t), as well as the structural variation of the chain. Here, U mainly refers to the Coulomb interaction between two electrons when they occupy the same energy level with the opposite spin. Therefore it is also called the spin pairing energy; t specifically refers to the π - π interaction between TCNQs, the magnitude of which scale the delocalized level of electrons in the 1D TCNQ chains. Based on the tight-binding band approximation, when $U < 4t$, the 1D chain adopts a metallic band structure in which the band is one-quarter filled, as shown in Fig. 6(b). Further, when the TCNQ^{-0.5} lattice in the chain undergoes tetramerization, the energy gap appears with a $2k_F$ charge density wave (CDW) for lowering the total energy of the system and the crystal becomes semiconducting, as shown in Fig. 6(c). In the STM

images of Fig. 5, the tunneling contrast periodicity along the direction of the TCNQ chain (c axis) is consistent with the corresponding crystallographic parameter that is the $2k_F$ tetramerized structure in the bulk crystal of TEA(TCNQ)₂ and HEM(TCNQ)₂.^{16,20} As the STM image is composed of mainly the local density of states (LDOS) near E_F , the observed LDOS represents a commensurate CDW. Note that the tetramer structure has an inner molecular height corrugation that results from the slipped ring-external bond arrangement of TCNQ^{-0.5} anions [Fig. 4(b)], but the contrast in STM images along the c axis has not reflected this feature in every bright lobe. This indicates that the geometric structure of the 1D chain contributes less to the contrast of the STM image.

Large electron-electron repulsion (U) will suppress the tendency to form tetramers in a TCNQ^{-0.5} chain, with the consequence that a dimerized structure ($4k_F$) will be preferred. Previous studies on DPA(TCNQ)₂ indicate that the electric and magnetic phase transition occurs simultaneously at 215 K, which is indicative of spin-Peierls transition.^{18,19} As shown in Fig. 6(d), if $U > 4t$, a spin-polarized state can take place. The energy of this state can be further lowered by formation of a magnetic $4k_F$ structure which results in dimerization of the 1D chain, lowering the electron kinetic energy, and the formation of a band gap [Fig. 6(e)]. The STM image of DPA(TCNQ)₂ (Fig. 4) shows clearly the dimerized structure of the TCNQ^{-0.5} chain. In contrast to TEA(TCNQ)₂ and HEM(TCNQ)₂, the mechanism by which the strong electronic correlation (U is large) in DPA(TCNQ)₂ occurs has not been well clarified, which is ascribed, in general, to the influence of cations on the quasi-1D TCNQ^{-0.5} chains.

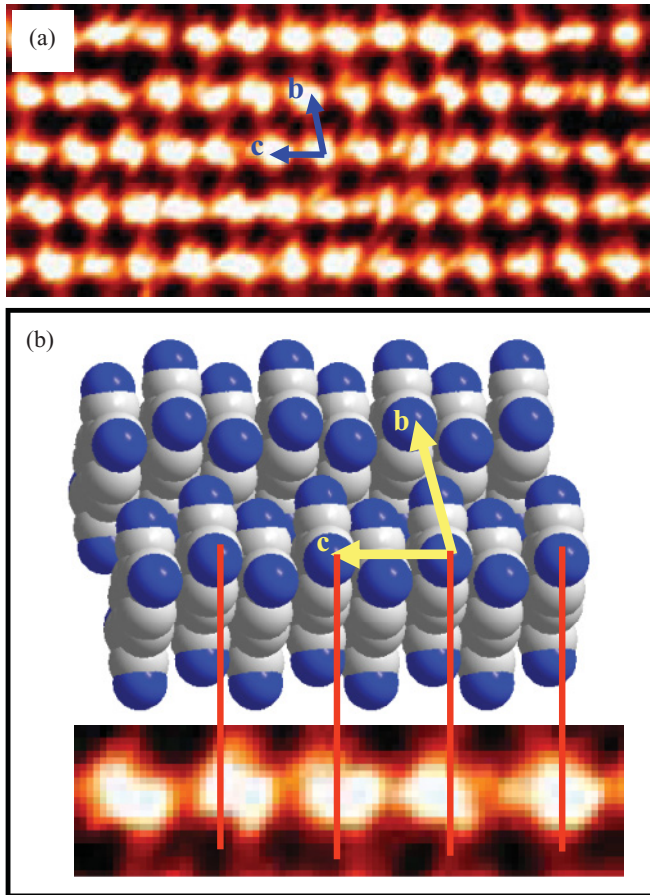


FIG. 4. (Color online) (a) High-resolution STM image of the *bc* surface of $\text{DPA}(\text{TCNQ})_2$ ($V_t = 40$ mV, $I_t = 0.3$ nA, 10.5×4.5 nm²), which is recognized as $\text{TCNQ}^{-0.5}$ terminated. The crystal axes of (b) and (c) are drawn in the image. (b) Space-filling model displaying the arrangement of the outermost $\text{TCNQ}^{-0.5}$ s of the *bc* surface, which was constructed through x-ray diffraction data. For a comparison, a segment of STM image cut from (a) was placed under the model with the same scale.

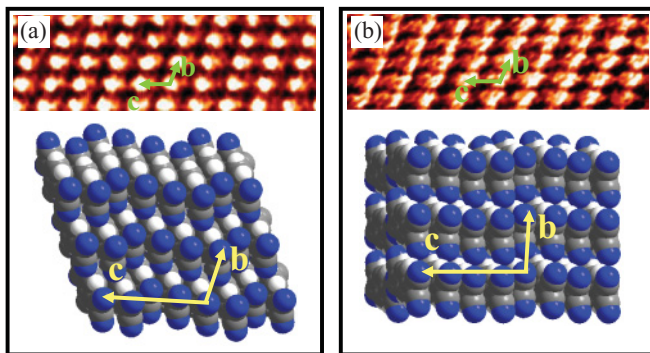


FIG. 5. (Color online) High-resolution STM images of the *bc* surface terminated with $\text{TCNQ}^{-0.5}$ s for (a) $\text{TEA}(\text{TCNQ})_2$ and (b) $\text{HEM}(\text{TCNQ})_2$, respectively, and space-filling models displaying the arrangement of the outermost $\text{TCNQ}^{-0.5}$ s of the *bc* surface were placed under the corresponding STM images. The scanning area is 12.5×4.0 nm², V_t is 50 mV, I_t is 0.3 nA. The crystal axes of (b) and (c) are drawn in the image.

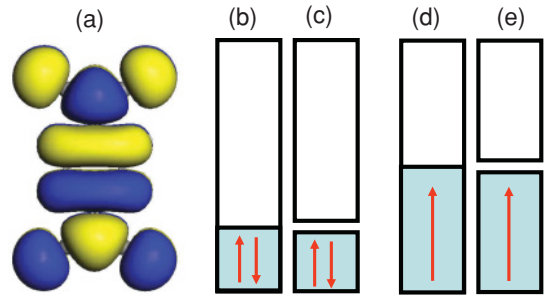


FIG. 6. (Color online) (a) LUMO of the TCNQ molecule. Schematic representation of the electron occupation in the energy band of a quasi-1D TCNQ chain formed by the LUMO, (b) metallic state one-quarter filled, (c) tetramerized $2k_F$ state, (d) polarized-spin state, and (e) dimerized $4k_F$ state.

Organic low-dimensional materials attract much attention due to the extensive π -electron delocalization along 1D or 2D stacks of anions or cations.² Some of these materials become superconductors. In general, these materials occur via Peierls or spin-Peierls transitions, which are usually derived by x-ray or neutron diffractions. Our STM images clearly visualize the structural character of these quasi-1D organic molecular chains in real space, which verifies that these phase transitions do happen in these organic materials.

D. Submolecular-resolution DPA^{+-} , TEA^{+-} , HEM^{+-} -terminated surfaces

Figure 7 shows STM images of the DPA^{+-} -terminated *bc* surface of the $\text{DPA}(\text{TCNQ})_2$ crystal, where two kinds of structures, the compact [Fig. 7(a)] and loose [Fig. 7(c)], exist with the following structural parameters: (i) $b = 0.51$ nm, $c = 1.0$ nm, $\gamma = 85.7^\circ$; (ii) $b = 0.70$ nm, $c = 1.16$ nm, $\gamma = 68.6^\circ$. These structure parameters are independent of the bulk crystallographic ones (Table I). During STM scanning, the two structures are easily exchanged due to the STM tip disturbance, indicative of their instability. Figures 7(b) and 7(d) are the enlarged images of the two structures with DPA^{+} molecules superimposed on the image

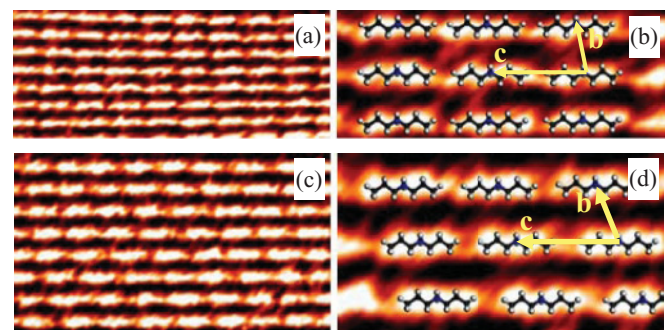


FIG. 7. (Color online) High-resolution STM images of the *bc* surface terminated with DPA^{+} s for (a) the compact structure and (b) the enlarged images with the DPA^{+} overlaid on the features; (c) the loose structure and (d) the enlarged images with the DPA^{+} overlaid on the features. The scanning areas of (a) and (c) are 9.5×4.0 nm² and 9.5×5.5 nm², respectively. The crystal axes of (b) and (c) are drawn in the image.

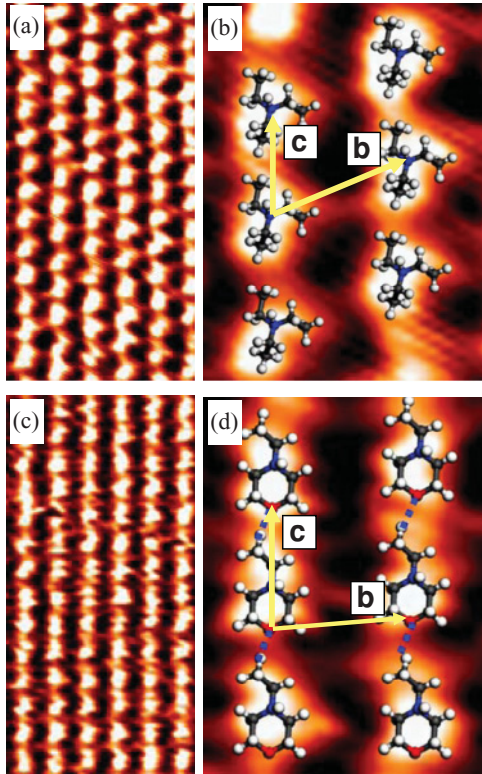


FIG. 8. (Color online) High-resolution STM images of the bc surface terminated with (a) TEA^+ s and (c) HEM^+ s. [(b) and (d)] The corresponding enlarged images with the TEA^+ and HEM^+ overlying the features, respectively. The scanning area of (a) and (c) is $10.5 \times 5.2 \text{ nm}^2$. The crystal axes of (b) and (c) are drawn in the image.

features. The shape of the image feature coincides very well with the profile of the overlaid molecules, clearly indicating that this surface is indeed terminated by DPA^+ . The ordering of the DPA^+ -terminated surface may arise from two factors: one is the long-range repulsion interaction between DPA^+ s that is very weak because the distance of neighboring DPA^+ s is very large. This is why the two structures are unstable. The other is that the DPA^+ may interact with the underlying $\text{TCNQ}^{-0.5}$ anions. In bulk, the interaction between DPA^+ and $\text{TCNQ}^{-0.5}$ is mainly via the hydrogen bond. But the surface DPA^+ , due to its conformation varying greatly from the bulk one, must give rise to the different interaction with the underlying $\text{TCNQ}^{-0.5}$ anions from that within bulk. The structural instability described above implies that this interaction is also not strong. On all accounts, the exposed surface layer of DPA^+ , with its interaction environment differing greatly from the bulk one, adopts new structures, as observed in Fig. 7.

The DPA^+ cation, however, are in closed-shell configuration and are not likely to possess states in the vicinity of E_F . Therefore, the STM contrast largely comes from the individual molecular structural corrugation, which explains the similarity between the STM image and the profile of DPA^+ . Meanwhile the surface layer of DPA^+ blocks the STM tip to probe the LDOS of the underlying TCNQ layer.

Figure 8 shows STM images of TEA^+ - [Fig. 8(a)] and HEM^+ - [Fig. 8(c)] terminated bc surfaces of the $\text{TEA}(\text{TCNQ})_2$

and $\text{HEM}(\text{TCNQ})_2$ crystals, respectively. The unit cell measured from the images is $b = 1.02 \text{ nm}$, $c = 0.77 \text{ nm}$, $\gamma = 65.5^\circ$ for $\text{TEA}(\text{TCNQ})_2$ and $b = 0.87 \text{ nm}$, $c = 0.73 \text{ nm}$, $\gamma = 86.8^\circ$ for $\text{HEM}(\text{TCNQ})_2$. These parameters also differ largely from those of the bulk ones listed in Table I. Figures 8(b) and 8(d) are the enlarged images of the two bc surfaces with TEA^+ and HEM^+ superimposed on the image features, respectively. The shape of the image feature coincides very well with the profile of the overlaid cations, clearly indicating that the surfaces are indeed terminated by TEA^+ and HEM^+ , respectively. In comparison to the DPA^+ -terminated surface, the TEA^+ - and HEM^+ -terminated surfaces are more stable during STM scanning. In particular, by repeatedly scanning the HEM^+ -terminated surface, the same STM images were achieved without any change in structure. In consideration of an oxygen atom in the HEM molecule, the distance of the oxygen atom and the CH group on the neighboring HEM molecule, as marked in the dotted lines in Fig. 8(d), is about 1.8 \AA , which falls into the interacting range of a hydrogen bond $\text{CH} \cdots \text{O}$.²⁵ Therefore, the formation of the hydrogen bond enhances the structural stability on the HEM^+ -terminated surface.

The STM results of the cation-terminated bc surfaces show that the surface structures deviate greatly from the corresponding ones, indicative of self-reassembling of these surface cations. This can be ascribed to the fact that the interactions between surface cations and the underlying layer are weak bonds, such as van der Waals forces or hydrogen bonds, which are easily altered in surface environments that differ from the bulk one. Also, the specific chemical structure of these cations is an important factor that influences the formed surface structure and stability.

IV. CONCLUSION

The anion- ($\text{TCNQ}^{-0.5}$) and cation- (DPA^+ , TEA^+ , HEM^+) terminated bc surfaces for the quasi-1D charge-transfer-complex organic crystals $\text{DPA}(\text{TCNQ})_2$, $\text{TEA}(\text{TCNQ})_2$, and $\text{HEM}(\text{TCNQ})_2$ have been revealed by STM, which exhibit the distinct characteristics of surface structure. The $\text{TCNQ}^{-0.5}$ -terminated bc surfaces of the three crystals strictly maintain the same lattice periodicity as the bulk crystallographic parameters, and the LDOS detected by STM represent a commensurate $2k_F$ [$\text{TEA}(\text{TCNQ})_2$ and $\text{HEM}(\text{TCNQ})_2$] or $4k_F$ [$\text{DPA}(\text{TCNQ})_2$] CDW that occurs at the quasi-1D $\text{TCNQ}^{-0.5}$ chain in bulk materials. Such structural rigidity is a consequence of the strong π - π overlapping interaction between $\text{TCNQ}^{-0.5}$ s within a chain. For cation-terminated bc surfaces, the surface lattice constants deviate greatly from the corresponding ones, implying a self-reassembling of surface structures. This behavior is attributed to the weak interactions between cations or with the underlying layer that are more sensitive to the variation of interaction environments.

ACKNOWLEDGMENTS

This work was supported by NSFC (60977015, 61076009, 60736034) and MOST (2007CB936800).

*zhuxing@pku.edu.cn

- ¹J. Ferraris, D. O. Cowan, V. Walatka, and J. H. Perlstein, *J. Am. Chem. Soc.* **95**, 948 (1973).
- ²R. P. Shibaeva and E. B. Yagubskii, *Chem. Rev.* **104**, 5347 (2004).
- ³M. Chollet, L. Guerin, N. Uchida, S. Fukaya, H. Shimoda, T. Ishikawa, K. Matsuda, T. Hasegawa, A. Ota, H. Yamochi, G. Saito, R. Tazaki, S. Adachi, and S. Koshihara, *Science* **307**, 86 (2005).
- ⁴F. Lin, W. Zhou, X. M. Huang, L. Ren, and Z. F. Liu, *J. Phys. Chem. C* **112**, 1090 (2008).
- ⁵E. Coronado and P. Day, *Chem. Rev.* **104**, 5419 (2004).
- ⁶K. Xiao, I. N. Ivanov, A. A. Puzetzy, Z. Liu, and D. B. Geohegan, *Adv. Mater.* **18**, 2184 (2006).
- ⁷H. L. Peng, C. B. Ran, X. C. Yu, R. Zhang, and Z. F. Liu, *Adv. Mater.* **17**, 459 (2005).
- ⁸A. Ota, H. Yamochi, and G. J. Saito, *Mater. Chem.* **12**, 2600 (2002).
- ⁹S. S. P. Parkin, M. Miljak, and J. R. Cooper, *Phys. Rev. B* **34**, 1485 (1986).
- ¹⁰T. Iizuka-Sakano, T. Kawamoto, Y. Shimoi, and S. Abe, *Phys. Rev. B* **70**, 085111 (2004).
- ¹¹R. T. Clay, S. Mazumdar, and D. K. Campbell, *Phys. Rev. B* **67**, 115121 (2003).
- ¹²S. Mazumdar, R. T. Clay, and D. K. Campbell, *Phys. Rev. B* **62**, 13400 (2000).
- ¹³P. Monceau, F. Y. Nad, and S. Brazovskii, *Phys. Rev. Lett.* **86**, 4080 (2001).
- ¹⁴M. Ishida, T. Mori, and H. Shigekawa, *Phys. Rev. Lett.* **83**, 596 (1999).
- ¹⁵H. Shigekawa, K. Miyake, A. Miyauchi, M. Ishida, H. Oigawa, Y. Nannichi, R. Yoshizaki, and T. Mori, *Phys. Rev. B* **52**, 16361 (1995).
- ¹⁶A. Filhol and M. Thomas, *Acta Cryst. B* **40**, 44 (1984).
- ¹⁷R. J. J. Visser, S. Oostra, C. Vettier, and J. Voiron, *Phys. Rev. B* **28**, 2074 (1983).
- ¹⁸K. D. Truong, C. Pépin, A. D. Bandrauk, M. Drouin, A. Michel, and M. Banville, *Can. J. Chem.* **69**, 1804 (1991).
- ¹⁹A. D. Bandrauk, K. D. Truong, and M. Aubin, *Can. J. Chem.* **66**, 938 (1988).
- ²⁰B. V. Bodegom and J. L. D. Boer, *Acta Crystallogr.* **37**, 119 (1981).
- ²¹C. B. Ran, H. L. Peng, L. Ren, W. Zhou, Y. D. Ling, and Z. F. Liu, *J. Phys. Chem. C* **111**, 631 (2007).
- ²²X. C. Yu, H. L. Peng, C. B. Ran, L. Sun, R. Zhang, and Z. F. Liu, *Appl. Phys. Lett.* **86**, 033105 (2005).
- ²³H. L. Peng, Z. Chen, L. M. Tong, X. C. Yu, C. B. Ran, and Z. F. Liu, *J. Phys. Chem. B* **109**, 3526 (2005).
- ²⁴L. R. Melby, R. J. Harder, W. R. Hertler, W. Mahler, R. E. Benson, and W. E. Mochel, *J. Am. Chem. Soc.* **84**, 3374 (1962).
- ²⁵G. A. Jeffrey, *An Introduction to Hydrogen Bonding* (Oxford University Press, Oxford, UK, 1997).